Lowest order Virtual Element approximation of magnetostatic problems

L. Beirão da Veiga[a,b], F. Brezzi[b,*], F. Dassi[a], L.D. Marini[c,b], A. Russo[a,b]

[a] *Dipartimento di Matematica e Applicazioni, Università di Milano–Bicocca, Via Cozzi 53, I-20153, Milano, Italy*
[b] *IMATI CNR, Via Ferrata 1, I-27100 Pavia, Italy*
[c] *Dipartimento di Matematica, Università di Pavia, Via Ferrata 5, I-27100 Pavia, Italy*

Abstract

We give here a simplified presentation of the lowest order Serendipity Virtual Element method, and show its use for the numerical solution of linear magneto-static problems in three dimensions. The method can be applied to very general decompositions of the computational domain (as is natural for Virtual Element Methods) and uses as unknowns the (constant) tangential component of the magnetic field $\boldsymbol{H}$ on each edge, and the vertex values of the Lagrange multiplier p (used to enforce the solenoidality of the magnetic induction $\boldsymbol{B} = \mu\boldsymbol{H}$). In this respect the method can be seen as the natural generalization of the lowest order Edge Finite Element Method (the so-called "first kind Nédélec" elements) to polyhedra of almost arbitrary shape, and as we show on some numerical examples it exhibits very good accuracy (for being a lowest order element) and excellent robustness with respect to distortions.

Keywords: Finite Element Methods, Virtual Element Methods, Magnetostatic problems, Serendipity.
AMS Subject Classification: 65N30

1. Introduction

In this paper we introduce a simplified version of the Serendipity Virtual Element Methods (VEMs) presented in [9] and [10] and we show how they can be used for the numerical solution of linear magneto-static problems in the so-called Kikuchi formulation (see e.g. [21]).

Serendipity VEMs are a recent variant of Virtual Element Methods that allow (as is the case of classical Serendipity Finite Elements (FEMs) on quadrilaterals and hexahedra) to eliminate a certain number of degrees of freedom (internal to faces and volumes) without compromising the order of accuracy. In the Virtual Element framework they are particularly useful since the original formulations of VEMs (as in [6] or [8]) often use more degrees of freedom than their FEM counterpart (when it exists).

The advantage of VEMs, when it comes to Serendipity variants, is that, contrary to FEMs, they do not use a reference element: an inevitable sacrifice, if you want to be able to deal with very general geometries.

*Corresponding author
Email addresses: lourenco.beirao@unimib.it (L. Beirão da Veiga), brezzi@imati.cnr.it (F. Brezzi), franco.dassi@unimib.it (F. Dassi), marini@imati.cnr.it (L.D. Marini), alessandro.russo@unimib.it (A. Russo)

Such a sacrifice, that requires additional computations on the current element, has however the advantage of being much more robust with respect to distortions, whereas Serendipity FEMs can lose orders of accuracy already on innocent quadrilaterals that are not parallelograms (as is well known, and has been analyzed e.g. in [2], [3]).

Here, as we said, we present a variant of the general theories of [9] and [10], that is specially designed for *lowest order* cases and comes out to be simpler, both for the theoretical presentation and the practical implementation.

Then we apply it to the classical *model* magnetostatic problem, in a *smooth-enough* simply connected bounded domain Ω in $\mathbb{R}^3$:

$$\begin{cases} \text{given } \boldsymbol{j} \in H(\mathrm{div};\Omega) \quad (\text{with } \mathrm{div}\boldsymbol{j} = 0 \text{ in } \Omega), \quad \text{and } \mu = \mu(\boldsymbol{x}) \geq \mu_0 > 0, \\ \text{find } \boldsymbol{H} \in H(\mathbf{curl};\Omega) \text{ and } \boldsymbol{B} \in H(\mathrm{div};\Omega) \text{ such that:} \\ \mathbf{curl}\boldsymbol{H} = \boldsymbol{j} \text{ and } \mathrm{div}\boldsymbol{B} = 0, \text{ with } \boldsymbol{B} = \mu\boldsymbol{H} \text{ in } \Omega \\ \text{with the boundary conditions } \boldsymbol{H} \wedge \boldsymbol{n} = 0 \text{ on } \partial\Omega. \end{cases} \tag{1.1}$$

In particular we shall deal with the variational formulation introduced in [21], that reads

$$\begin{cases} \text{find } \boldsymbol{H} \in H_0(\mathbf{curl};\Omega) \text{ and } p \in H_0^1(\Omega) \text{ such that:} \\ \displaystyle\int_\Omega \mathbf{curl}\boldsymbol{H} \cdot \mathbf{curl}\boldsymbol{v}\,\mathrm{d}\Omega + \int_\Omega \nabla p \cdot \mu\boldsymbol{v}\,\mathrm{d}\Omega = \int_\Omega \boldsymbol{j} \cdot \mathbf{curl}\boldsymbol{v}\,\mathrm{d}\Omega \quad \forall \boldsymbol{v} \in H_0(\mathbf{curl};\Omega) \\ \displaystyle\int_\Omega \nabla q \cdot \mu\boldsymbol{H}\,\mathrm{d}\Omega = 0 \quad \forall q \in H_0^1(\Omega). \end{cases} \tag{1.2}$$

For many other different approaches to the same problem see e.g. [23], [18], [13] and the references therein.

In our discretization, the scalar variable p (Lagrange multiplier for the condition $\mathrm{div}(\mu\boldsymbol{H}) = 0$) will be discretized using only vertex values as degrees of freedom, and the magnetic field $\boldsymbol{H}$ will be discretized using only one degree of freedom (= constant tangential component) per edge. In its turn the current $\boldsymbol{j}$ (here a given quantity) will be discretized by its lowest order *Face Virtual Element interpolant* $\boldsymbol{j}_I$, individuated by its constant normal component on each face.

On tetrahedrons this would correspond to use a piecewise linear scalar for p, a lowest-order Nédélec of the *first kind* for $\boldsymbol{H}$, and a lowest order Raviart-Thomas for $\boldsymbol{j}$: in a sense, nothing new. But already on prisms, pyramids, or hexahedra we start gaining, as we can allow more general geometries and more dramatic distortions, and there are no difficulties in using much more general polyhedrons.

On polyhedrons the present approach could also be seen as being close to previous works on Mimetic Finite Differences (the ancestor of Virtual Elements) like [16] or [22]. Here however the approach is more simple and direct, allowing a thorough analysis of convergence properties. Also the use of an explicit stabilizing term, reminiscent of Hybrid Discontinuous Galerkin methods (see e.g. [17] and the references therein) contributes, in our opinion, to the user-friendliness of the presentation.

A layout of the paper is as follows. The next section will be dedicated to recall the basic notation of functional spaces and differential operators.

Then in Section 3 we will introduce and discuss the two-dimensional VEMs (*nodal* and *edge*) that will be used on the faces of the three-dimensional decompositions. As usual, we will present first the spaces on a single two dimensional element (*local spaces*).

In Section 4 we will finally present our "Simplified Serendipity Spaces" in three dimensions. We first deal with a single element (polyhedron) and then discuss the spaces on a general decomposition.

In Section 5 we will use these spaces to discretize the linear magneto-static problem, and briefly discuss their convergence and the a-priori error analysis.

Finally, in Section 6 we will present some numerical results.

2. Notation

In any dimension, for an integer $s \geq -1$ we will denote by $\mathbb{P}_s$ the space of polynomials of degree $\leq s$. Following a common convention, $\mathbb{P}_{-1} \equiv \{0\}$ and $\mathbb{P}_0 \equiv \mathbb{R}$. Moreover, $\Pi_{s,\mathcal{O}}$ will denote the $L^2(\mathcal{O})$-orthogonal projection onto $\mathbb{P}_s$ (or $(\mathbb{P}_s)^2$, or $(\mathbb{P}_s)^3$). When no confusion can occur, this will be simply denoted by Π_s.

2.1. Basic notation in 2 and 3 dimensions

In two and three dimensions we will denote by $\boldsymbol{x}$ the indipendent variable. In two dimensions we will also use $\boldsymbol{x} = (x, y)$ or (more often) $\boldsymbol{x} = (x_1, x_2)$ following the circumstances. We will also use

$$\boldsymbol{x}^\perp := (-x_2, x_1) \tag{2.1}$$

In two dimensions, for a vector $\boldsymbol{v}$ and a scalar q we will write

$$\mathrm{rot}\boldsymbol{v} := \frac{\partial v_2}{\partial x} - \frac{\partial v_1}{\partial y}, \qquad \mathbf{rot}\, q := (\frac{\partial q}{\partial y}, -\frac{\partial q}{\partial x})^T. \tag{2.2}$$

We observe that

$$\mathrm{div}(p_0\boldsymbol{x}) = \mathrm{rot}(p_0\boldsymbol{x}^\perp) = 2p_0, \qquad \forall p_0 \in \mathbb{R}. \tag{2.3}$$

The following decompositions of polynomial vector spaces are well known and will be useful in what follows. In two dimensions we have, for all $s \geq 0$:

$$(\mathbb{P}_s)^2 = \mathbf{rot}\mathbb{P}_{s+1} \oplus \boldsymbol{x}\mathbb{P}_{s-1} \quad \text{and} \quad (\mathbb{P}_s)^2 = \mathbf{grad}\mathbb{P}_{s+1} \oplus \boldsymbol{x}^\perp\mathbb{P}_{s-1}. \tag{2.4}$$

In three dimensions the analogues of (2.4) (always for all $s \geq 0$) are

$$(\mathbb{P}_s)^3 = \mathbf{curl}((\mathbb{P}_{s+1})^3) \oplus \boldsymbol{x}\mathbb{P}_{s-1}, \quad \text{and} \quad (\mathbb{P}_s)^3 = \mathbf{grad}(\mathbb{P}_{s+1}) \oplus \boldsymbol{x} \wedge (\mathbb{P}_{s-1})^3. \tag{2.5}$$

We also note that by direct computation we have, similarly to (2.3):

$$\mathrm{div}(p_0\boldsymbol{x}) = 3p_0 \quad \forall p_0 \in \mathbb{P}_0 \qquad \text{and} \qquad \mathbf{curl}(\boldsymbol{p}_0 \wedge \boldsymbol{x}) = 2\boldsymbol{p}_0 \quad \forall \boldsymbol{p}_0 \in (\mathbb{P}_0)^3. \tag{2.6}$$

Finally, on a polyhedron P we set $\boldsymbol{x}_{\mathrm{P}} = \boldsymbol{x} - \mathbf{b}_{\mathrm{P}}$ with $\mathbf{b}_P$ the barycenter of P. Analogously, for each face $f \in \partial\mathrm{P}$, we set $\boldsymbol{x}_f = \boldsymbol{x} - \mathbf{b}_f$, with $\mathbf{b}_f$ = barycenter of f. Note that clearly

$$\int_{\mathrm{P}} \boldsymbol{x}_{\mathrm{P}} \,\mathrm{dP} = 0, \tag{2.7}$$

as well as

$$\int_f \boldsymbol{x}_f \,\mathrm{d}f = 0. \tag{2.8}$$

2.2. Polynomial spaces: Raviart-Thomas and Nédélec

We recall the definition of the classical lowest order Raviart-Thomas *local* spaces in d space dimensions

$$RT_0 = (\mathbb{P}_0)^d \oplus \boldsymbol{x}\,\mathbb{P}_0, \tag{2.9}$$

and also the classical lowest order Nédélec first-type *local* spaces in two and three space dimensions

$$N_0 = (\mathbb{P}_0)^2 \oplus \boldsymbol{x}^{\perp}\,\mathbb{P}_0 \quad \text{or} \quad N_0 = (\mathbb{P}_0)^3 \oplus \boldsymbol{x} \wedge (\mathbb{P}_0)^3. \tag{2.10}$$

In what follows, when dealing with the *faces* of a polyhedron (or of a polyhedral decomposition) we shall use two-dimensional differential operators that act on the restrictions to faces of scalar functions that are defined on a three-dimensional domain. Similarly, for vector valued functions we will use two-dimensional differential operators that act on the restrictions to faces of the tangential components. In many cases, no confusion will be likely to occur; however, to stay on the safe side, we will often use a superscript τ to denote the tangential components of a three-dimensional vector, and a subscript f to indicate the two-dimensional differential operator. Hence, to fix ideas, if a face has equation $x_3 = 0$ then $\boldsymbol{x}^{\tau} := (x_1, x_2)$ and, say, $\mathrm{div}_f \boldsymbol{v}^{\tau} := \frac{\partial v_1}{\partial x_1} + \frac{\partial v_2}{\partial x_2}$.

2.3. Some Functional Spaces

We recall some commonly used functional spaces:

$$\begin{aligned}
&H(\mathrm{div};\Omega) = \{\boldsymbol{v} \in [L^2(\Omega)]^3 \text{ with } \mathrm{div}\boldsymbol{v} \in L^2(\Omega)\},\\
&H_0(\mathrm{div};\Omega) = \{\boldsymbol{\varphi} \in H(\mathrm{div};\Omega) \text{ with } \boldsymbol{\varphi}\cdot\boldsymbol{n} = 0 \text{ on } \partial\Omega\},\\
&H(\mathbf{curl};\Omega) = \{\boldsymbol{v} \in [L^2(\Omega)]^3 \text{ with } \mathbf{curl}\boldsymbol{v} \in [L^2(\Omega)]^3\},\\
&H_0(\mathbf{curl};\Omega) = \{\boldsymbol{v} \in H(\mathbf{curl};\Omega) \text{ with } \boldsymbol{H}\wedge\boldsymbol{n} = 0 \text{ on } \partial\Omega\},\\
&H^1(\Omega) = \{q \in L^2(\Omega) \text{ with } \mathbf{grad}q \in (L^2(\Omega))^2\},\\
&H^1_0(\Omega) = \{q \in H^1(\Omega) \text{ with } q = 0 \text{ on } \partial\Omega\}.
\end{aligned}$$

3. Two-dimensional Simplified Serendipity Spaces

We begin with the definition of the local spaces. Let P denote a generic polyhedron, and let f be a face of such polyhedron. For the time being, we only assume that all faces f are simply connected.

3.1. The local spaces on faces

The following spaces are a simplified version of the local lowest-order *nodal* and *edge* Serendipity spaces on faces introduced in [7].

3.2. The local nodal space on faces

The present local *nodal* Virtual Element space on faces can be seen as an extension to polygons of the simplest space of piecewise linear functions on triangles, as well as a simplified version of the basic VEM nodal spaces.

Indeed, in [9] (formula (2.5) with $k = 1$, $k_\Delta = 0$) the basic lowest order local nodal space on faces was introduced as

$$\widetilde{V}_1^{\mathrm{node}}(f) := \Big\{ q \in C^0(f) :\ q_{|e} \in \mathbb{P}_1(e)\ \forall e \in \partial f,\ \Delta q \in \mathbb{P}_0(f) \Big\}. \tag{3.1}$$

It is clear that we always have $\mathbb{P}_1 \subset \widetilde{V}_1^{\mathrm{node}}(f)$. The original degrees of freedom proposed in [6] or in [1] were

- The values of q at the vertices (that is : for each vertex ν, the value $q(\nu)$); (3.2)
- The mean value of q on f (that is: for each face f, $\dfrac{1}{|f|}\displaystyle\int_f q \,\mathrm{d}f$). (3.3)

However, it was pointed out in [7] that the degrees of freedom (3.3) could be replaced by the integral

$$\int_f \nabla q \cdot \boldsymbol{x}_f \,\mathrm{d}f. \tag{3.4}$$

Indeed, the obvious identity

$$2\int_f q \,\mathrm{d}f = \int_f q \,\mathrm{div}\boldsymbol{x}_f \,\mathrm{d}f = -\int_f \nabla q \cdot \boldsymbol{x}_f \,\mathrm{d}f + \int_{\partial f} q \boldsymbol{x}_f \cdot \boldsymbol{n} \,\mathrm{d}s \tag{3.5}$$

shows that given boundary values and mean value (3.3) on f one can compute (3.4) and conversely, given the boundary values and (3.4) one can compute the mean value on f.

At this point, remembering (2.8), we easily see that

$$\int_f \nabla q \cdot \boldsymbol{x}_f \,\mathrm{d}f = 0 \qquad \forall q \in \mathbb{P}_1, \tag{3.6}$$

so that the linear subspace of $\widetilde{V}_1^{\mathrm{node}}(f)$ made of those q that verify (3.6) will still contain $\mathbb{P}_1$. Such a subspace can obviously be written as

$$V_1^{\mathrm{node}}(f) := \Big\{ q \in C^0(f) : q_{|e} \in \mathbb{P}_1(e)\ \forall e \in \partial f,\ \Delta q \in \mathbb{P}_0(f), \int_f \nabla q \cdot \boldsymbol{x}_f \,\mathrm{d}f = 0 \Big\}, \tag{3.7}$$

and will be our local *scalar nodal VEM space*, with the degrees of freedom (3.2) (i.e., the vertex values). Then from the unisolvence of the degrees of freedom (3.2) and (3.3) in $\widetilde{V}_1^{\mathrm{node}}(f)$ it follows rather obviously that the degrees of freedom (3.2) are unisolvent in $V_1^{\mathrm{node}}(f)$. Indeed: for a $q \in V_1^{\mathrm{node}}(f)$, the degrees of

freedom (3.2) give the value of q along the whole ∂f. Then, following (3.5), and using the information that $\int_f \nabla q \cdot \boldsymbol{x}_f \, \mathrm{d}f = 0$ (that is included in the definition (3.7) of $q \in V_1^{\mathrm{node}}(f)$) we have

$$2 \int_f q \, \mathrm{d}f = \int_{\partial f} q \, \boldsymbol{x}_f \cdot \boldsymbol{n} \, \mathrm{d}s, \tag{3.8}$$

and then from the boundary values of q we can easily compute the mean value of q on f. Now we know both the degrees of freedom (3.2) *and* (3.3), and we are back on the track of the space $\widetilde{V}_1^{\mathrm{node}}(f)$.

We point out that, if needed, out of the d.o.f. in (3.2) we can compute the L^2-projection Π_1 of ∇q onto $(\mathbb{P}_1)^2$. Indeed, from the definition of projection and (3.5) we deduce

$$\int_f \Pi_1 \nabla q \cdot \boldsymbol{p}_1 \, \mathrm{d}f := \int_f \nabla q \cdot \boldsymbol{p}_1 \, \mathrm{d}f = -\int_f q \, \mathrm{div} \boldsymbol{p}_1 \, \mathrm{d}f + \int_{\partial f} q \, \boldsymbol{p}_1 \cdot \boldsymbol{n} \, \mathrm{d}s, \tag{3.9}$$

and the last two terms are computable for every $\boldsymbol{p}_1 \in (\mathbb{P}_1)^2$.

3.3. The local edge space on faces

The present local *edge* Virtual Element space on faces can be seen as an extension to polygons of the simplest space of lowest order Nédélec elements of the first kind N_0 (see (2.10)), as well as a simplified version of the basic VEM edge spaces in [7, 10].

Indeed, in [10] (formula (6.1) with $k = 0$, $k_d = 0$, $k_r = 0$) the basic lowest order local edge space on faces was introduced as

$$\widetilde{V}_0^{\mathrm{edge}}(f) := \Big\{ \boldsymbol{v} \in (L^2(f))^2 \, : \mathrm{div} \boldsymbol{v} \in \mathbb{P}_0(f), \, \mathrm{rot} \boldsymbol{v} \in \mathbb{P}_0(f), \boldsymbol{v} \cdot \boldsymbol{t}_e \in \mathbb{P}_0(e) \, \forall e \in \partial f \Big\}, \tag{3.10}$$

with the degrees of freedom given by the (constant) tangential components on each edge, plus the integral

$$\int_f \boldsymbol{v} \cdot \boldsymbol{x}_f \, \mathrm{d}f. \tag{3.11}$$

The space given in (3.10) clearly contains all constant vector fields. However, for these functions the degree of freedom (3.11) is identically zero (due to (2.8)). Hence we could consider the subspace

$$\begin{aligned} V_0^{\mathrm{edge}}(f) := \Big\{ \boldsymbol{v} \in (L^2(f))^2 \, : & \mathrm{div} \boldsymbol{v} \in \mathbb{P}_0(f), \, \mathrm{rot} \boldsymbol{v} \in \mathbb{P}_0(f), \boldsymbol{v} \cdot \boldsymbol{t}_e \in \mathbb{P}_0(e) \, \forall e \in \partial f, \\ & \text{and} \quad \int_f \boldsymbol{v} \cdot \boldsymbol{x}_f \, \mathrm{d}f = 0 \Big\}, \end{aligned} \tag{3.12}$$

that we will take, from now on, as our edge VEM space, and have that it always contains the constant vector fields. In $V_0^{\mathrm{edge}}(f)$ we will therefore have the degrees of freedom:

- on each $e \in \partial f$, the moments $\displaystyle\int_e \boldsymbol{v} \cdot \boldsymbol{t}_e \, \mathrm{d}e$. (3.13)

Note that the number of degrees of freedom of $V_1^{\mathrm{node}}(f)$ (=number of vertexes) and of $V_0^{\mathrm{edge}}(f)$ (=number of edges) obviously coincide.

Remark 1. *It is immediate to check that the space* (3.12) *contains, together with constant vector fields, also all vector fields of the form* $\boldsymbol{v} = \boldsymbol{p}_0 + \boldsymbol{x}_f^{\perp} p_0$ *with* $\boldsymbol{p}_0 \in \mathbb{R}^2$ *and* $p_0 \in \mathbb{R}$ *(that is, the lowest order Nédélec elements of the first kind, that we recalled in* (2.10)*).* □

We observe that the d.o.f. (3.13) allow to compute, for each $\boldsymbol{v} \in V_0^{\text{edge}}(f)$, the (constant) value of $\text{rot}\boldsymbol{v}$ on the face f by the usual Stokes theorem

$$|f|\text{rot}\boldsymbol{v} = \int_f \text{rot}\boldsymbol{v}\,\mathrm{d}f = \int_{\partial f} \boldsymbol{v}\cdot\boldsymbol{t}\,\mathrm{d}s, \tag{3.14}$$

as well as the L^2-orthogonal projection $\Pi_1 : V_0^{\text{edge}}(f) \to (\mathbb{P}_1(f))^2$. Indeed, using (2.4) and integrating by parts we have

$$\begin{aligned}\int_f \Pi_1\boldsymbol{v}\cdot\boldsymbol{p}_1\,\mathrm{d}f &:= \int_f \boldsymbol{v}\cdot\boldsymbol{p}_1\,\mathrm{d}f = \int_f \boldsymbol{v}\cdot(\mathbf{rot}\,p_2 + \boldsymbol{x}_f p_0)\,\mathrm{d}f\\ &= \int_f \text{rot}\,\boldsymbol{v}\,p_2\,\mathrm{d}f + \int_{\partial f}\boldsymbol{v}\cdot\boldsymbol{t}\,p_2\,\mathrm{d}s + \int_f \boldsymbol{v}\cdot\boldsymbol{x}_f p_0\,\mathrm{d}f\\ &= \int_f \text{rot}\,\boldsymbol{v}\,p_2\,\mathrm{d}f + \int_{\partial f}\boldsymbol{v}\cdot\boldsymbol{t}\,p_2\,\mathrm{d}s,\end{aligned} \tag{3.15}$$

and all the terms in the right-hand side are computable.

We close this section with a simple but important result.

Proposition 3.1. *It holds*

$$\nabla V_1^{\text{node}}(f) = \{\boldsymbol{v}\in V_0^{\text{edge}}(f) :\ \text{rot}\boldsymbol{v} = 0\}. \tag{3.16}$$

Proof. We start by noting that, for any function $q \in V_1^{\text{node}}(f)$, it holds

$$\nabla q \in V_0^{\text{edge}}(f) \ \text{ and } \ \text{rot}\nabla q = 0.$$

Indeed, it is immediate to check that ∇q satisfies all the requirements in the definition of $V_0^{\text{edge}}(f)$ and, being a gradient, it also has vanishing rotor. Therefore

$$\nabla V_1^{\text{node}}(f) \subseteq \{\boldsymbol{v}\in V_0^{\text{edge}}(f) :\ \text{rot}\boldsymbol{v} = 0\},$$

that combined with

$$\begin{aligned}\dim\left(\nabla V_1^{\text{node}}(f)\right) &= \dim\left(V_1^{\text{node}}(f)\right) - 1 = \dim\left(V_0^{\text{edge}}(f)\right) - 1\\ &= \dim\Big(\{\boldsymbol{v}\in V_0^{\text{edge}}(f) :\ \text{rot}\boldsymbol{v} = 0\}\Big)\end{aligned}$$

yields the proof. □

4. Three-dimensional spaces

Let P be a polyhedron. For the time being, we just assume that P and all of its faces are simply connected. Let N_v be the number of vertices, N_e the number of edges, and N_f the number of faces of P.

4.1. The local spaces on polyhedrons

For each face f we are going to use the spaces $V_1^{\rm node}(f)$ and $V_0^{\rm edge}(f)$ as defined in (3.7) and (3.12), respectively. Then we introduce their three-dimensional analogues.

4.1.1. The local nodal spaces

The three dimensional local nodal space is defined as

$$V_1^{\rm node}({\rm P}) := \Big\{ q \in C^0({\rm P}) \ : q_{|f} \in V_1^{\rm node}(f) \ \forall \text{ face } f \in \partial{\rm P},\ \Delta\, q = 0 \text{ in P} \Big\}. \tag{4.1}$$

In $V_1^{\rm node}({\rm P})$ the degrees of freedom are simply

$$\bullet \text{ for each vertex } \nu, \text{ the nodal value } q(\nu). \tag{4.2}$$

We note that

$$\mathbb{P}_1({\rm P}) \subseteq V_1^{\rm node}({\rm P}),$$

since first order polynomials clearly satisfy all the conditions in (4.1).

4.1.2. The local edge spaces

In analogy with the two-dimensional case we start by recalling the three dimensional edge space defined in [10] as

$$\widetilde{V}_0^{\rm edge}({\rm P}) := \Big\{ \boldsymbol{v} \in (L^2({\rm P}))^3 \ : \boldsymbol{v}^\tau{}_{|f} \in V_0^{\rm edge}(f) \ \forall \text{ face } f \in \partial{\rm P},\ \boldsymbol{v}\cdot\boldsymbol{t}_e \text{ continuous at each edge } e \in \partial{\rm P}, \\ {\rm div}\boldsymbol{v} = 0 \text{ in P}, \ \mathbf{curl}(\mathbf{curl}\boldsymbol{v}) \in (\mathbb{P}_0({\rm P}))^3 \Big\}, \tag{4.3}$$

with the degrees of freedom given by the values of the (constant) tangential components on each edge plus the integrals

$$\int_{\rm P} (\mathbf{curl}\boldsymbol{v}) \cdot (\boldsymbol{x}_{\rm P} \wedge \boldsymbol{p}_0) \ {\rm dP} \quad \forall\, \boldsymbol{p}_0 \in (\mathbb{P}_0({\rm P}))^3. \tag{4.4}$$

We observe, first, that the constant vectors are contained in $\widetilde{V}_0^{\rm edge}({\rm P})$, and for them the integral in (4.4) is always equal to zero. Hence, following the path that is becoming usual here, we set

$$V_0^{\rm edge}({\rm P}) := \Big\{ \boldsymbol{v} \in (L^2({\rm P}))^3 \ : \boldsymbol{v}^\tau{}_{|f} \in V_0^{\rm edge}(f) \ \forall \text{ face } f \in \partial{\rm P},\ \boldsymbol{v}\cdot\boldsymbol{t}_e \text{ continuous at each edge } e \in \partial{\rm P}, \\ {\rm div}\boldsymbol{v} = 0 \text{ in P}, \ \mathbf{curl}(\mathbf{curl}\boldsymbol{v}) \in (\mathbb{P}_0({\rm P}))^3, \ \int_{\rm P} (\mathbf{curl}\boldsymbol{v}) \cdot (\boldsymbol{x}_{\rm P} \wedge \boldsymbol{p}_0) \ {\rm dP} = 0 \quad \forall \boldsymbol{p}_0 \in (\mathbb{P}_0({\rm P}))^3 \Big\}, \tag{4.5}$$

and observe that all the constant vector fields are contained in $V_0^{\rm edge}({\rm P})$.

Remark 2. *It is easy to check that the space* (4.5)*, together with constant vector fields, contains all vector fields of the form* $\boldsymbol{v} = \boldsymbol{p}_0 + \boldsymbol{x}_P \wedge \boldsymbol{q}_0$ *with* $\boldsymbol{p}_0$ *and* $\boldsymbol{q}_0$ *in* $\mathbb{R}^3$ *(that is, the lowest order Nédélec elements of the first kind in three dimensions, as defined in* (2.10)*).* □

In $V_0^{\text{edge}}(\mathrm{P})$ we have now the degrees of freedom,

$$\bullet \text{ on each edge } e \in \partial P \text{ the moments } \int_e \boldsymbol{v}\cdot\boldsymbol{t}_e \,\mathrm{d}e. \tag{4.6}$$

Out of the above degrees of freedom we can compute the $(L^2(\mathrm{P}))^3$-orthogonal projection Π_0 from $V_0^{\text{edge}}(\mathrm{P})$ to $(\mathbb{P}_0(\mathrm{P}))^3$. Indeed, by definition of projection, (2.6), and an integration by parts we have:

$$\begin{aligned}
\int_{\mathrm{P}} \Pi_0\boldsymbol{v}\cdot\boldsymbol{p}_0 \,\mathrm{d}\mathrm{P} &:= \int_{\mathrm{P}} \boldsymbol{v}\cdot\boldsymbol{p}_0 \,\mathrm{d}\mathrm{P} = \int_{\mathrm{P}} \boldsymbol{v}\cdot\mathbf{curl}(\boldsymbol{x}_{\mathrm{P}}\wedge\boldsymbol{q}_0)\,\mathrm{d}\mathrm{P} \ (\text{for } \boldsymbol{q}_0 = -\frac{1}{2}\boldsymbol{p}_0)\\
&= \int_{\mathrm{P}} \mathbf{curl}\boldsymbol{v}\cdot(\boldsymbol{x}_{\mathrm{P}}\wedge\boldsymbol{q}_0)\,\mathrm{d}\mathrm{P} + \int_{\partial\mathrm{P}} (\boldsymbol{v}\wedge\boldsymbol{n})\cdot(\boldsymbol{x}_{\mathrm{P}}\wedge\boldsymbol{q}_0)\,\mathrm{d}S\\
&= \qquad 0 \qquad\qquad + \int_{\partial\mathrm{P}} \Big(\boldsymbol{n}\wedge(\boldsymbol{x}_{\mathrm{P}}\wedge\boldsymbol{q}_0)\Big)\cdot\boldsymbol{v}\,\mathrm{d}S\\
&= \sum_f \int_f \Big(\boldsymbol{n}\wedge(\boldsymbol{x}_{\mathrm{P}}\wedge\boldsymbol{q}_0)\Big)^{\tau}\cdot\boldsymbol{v}^{\tau}\,\mathrm{d}f,
\end{aligned} \tag{4.7}$$

that is computable as in (3.15). Hence, we can define a scalar product

$$[\boldsymbol{v},\boldsymbol{w}]_{\text{edge},\mathrm{P}} := (\Pi_0\boldsymbol{v},\Pi_0\boldsymbol{w})_{0,\mathrm{P}} + h_{\mathrm{P}}^2 \sum_{e\in\partial\mathrm{P}} \int_e [(\boldsymbol{v}-\Pi_0\boldsymbol{v})\cdot\boldsymbol{t}_e]\,[(\boldsymbol{w}-\Pi_0\boldsymbol{w})\cdot\boldsymbol{t}_e]\,\mathrm{d}e \tag{4.8}$$

and we note that (assuming very mild mesh regularity conditions, for instance as in Section 5.1) we have

$$\alpha_*(\boldsymbol{v},\boldsymbol{v})_{0,\mathrm{P}} \le [\boldsymbol{v},\boldsymbol{v}]_{\text{edge},\mathrm{P}} \le \alpha^*(\boldsymbol{v},\boldsymbol{v})_{0,\mathrm{P}} \qquad \forall \boldsymbol{v}\in V_0^{\text{edge}}(\mathrm{P}) \tag{4.9}$$

for some constants α_*, α^* independent of h_{P}. We observe that

$$[\boldsymbol{v},\boldsymbol{p}_0]_{\text{edge},\mathrm{P}} = \int_{\mathrm{P}} \boldsymbol{v}\cdot\boldsymbol{p}_0\,\mathrm{d}\mathrm{P} = (\boldsymbol{v},\boldsymbol{p}_0)_{0,\mathrm{P}} \quad \forall \boldsymbol{v}\in V_0^{\text{edge}}(\mathrm{P}),\ \forall \boldsymbol{p}_0\in(\mathbb{P}_0(\mathrm{P}))^3. \tag{4.10}$$

4.1.3. The local face spaces

In three dimensions we will also need a Virtual Element face space. For it, we proceed as in the previous case. We start with the space defined in [10]

$$\widetilde{V}_0^{\text{face}}(\mathrm{P}) := \Big\{\boldsymbol{\psi}\in(L^2(\mathrm{P}))^3 : \boldsymbol{\psi}\cdot\boldsymbol{n}_f\in\mathbb{P}_0(f)\ \forall \text{ face } f,\ \mathrm{div}\boldsymbol{\psi}\in\mathbb{P}_0(\mathrm{P}),\ \mathbf{curl}\boldsymbol{\psi}\in(\mathbb{P}_0(\mathrm{P}))^3\Big\}, \tag{4.11}$$

where the degrees of freedom are given by the (constant) values of the normal components on the faces plus the value of the integrals:

$$\int_{\mathrm{P}} \boldsymbol{\psi}\cdot(\boldsymbol{x}_{\mathrm{P}}\wedge\boldsymbol{p}_0)\,\mathrm{d}\mathrm{P} \quad \forall \boldsymbol{p}_0\in[\mathbb{P}_0(\mathrm{P})]^3. \tag{4.12}$$

We note that the constant vector fields are inside this space, but also that the value of the integral in (4.12), for $\boldsymbol{\psi}$ constant, is always equal to zero, due to (2.7), so that we can define

$$\begin{aligned}
V_0^{\text{face}}(\mathrm{P}) := \Big\{\boldsymbol{\psi}\in(L^2(\mathrm{P}))^3 : \boldsymbol{\psi}\cdot\boldsymbol{n}_f\in\mathbb{P}_0(f)\ \forall \text{ face } f,\ \mathrm{div}\boldsymbol{\psi}\in\mathbb{P}_0(\mathrm{P}),\ \mathbf{curl}\boldsymbol{\psi}\in(\mathbb{P}_0(\mathrm{P}))^3,\\
\text{and } \int_{\mathrm{P}} \boldsymbol{\psi}\cdot(\boldsymbol{x}_{\mathrm{P}}\wedge\boldsymbol{p}_0)\,\mathrm{d}\mathrm{P} = 0 \quad \forall \boldsymbol{p}_0\in[\mathbb{P}_0(\mathrm{P})]^3\Big\}.
\end{aligned} \tag{4.13}$$

Remark 3. *It is easy to check that the space* (4.13)*, together with constant vector fields, contains all vector fields of the form* $(\mathbb{P}_0)^3 + \boldsymbol{x}_P\mathbb{P}_0$ *(that is, the lowest order Raviart-Thomas space, as defined in* (2.9)*).* □

For $V_0^{\text{face}}(\mathrm{P})$ we have therefore the degrees of freedom

$$\bullet \text{ for each face } f \in \partial P \text{ the moments } \int_f \boldsymbol{\psi}\cdot\boldsymbol{n}_f \,\mathrm{d}f. \tag{4.14}$$

Clearly, out of the degrees of freedom (4.14) we can easily compute the (constant) value of $\mathrm{div}\boldsymbol{\psi}$

$$\mathrm{div}\boldsymbol{\psi} = \frac{1}{|\mathrm{P}|}\int_{\mathrm{P}} \mathrm{div}\boldsymbol{\psi}\,\mathrm{dP} = \frac{1}{|\mathrm{P}|}\int_{\partial\mathrm{P}} \boldsymbol{\psi}\cdot\boldsymbol{n}\,\mathrm{d}S. \tag{4.15}$$

According to [10] we also have, now, that from the above degrees of freedom we can compute the $(L^2(\mathrm{P}))^3$-orthogonal projection from $V_0^{\text{face}}(\mathrm{P})$ to $(\mathbb{P}_0(\mathrm{P}))^3$ (and, actually, to $(\mathbb{P}_1(\mathrm{P}))^3$). Indeed, using (2.5), an integration by parts, and (4.13), we have:

$$\begin{aligned}\int_{\mathrm{P}} \Pi_1\boldsymbol{\psi}\cdot\boldsymbol{p}_1\,\mathrm{dP} &:= \int_{\mathrm{P}} \boldsymbol{\psi}\cdot\boldsymbol{p}_1\,\mathrm{dP} = \int_{\mathrm{P}} \boldsymbol{\psi}\cdot(\nabla p_2 + \boldsymbol{x}_{\mathrm{P}}\wedge\boldsymbol{p}_0)\,\mathrm{dP}\\ &= -\int_{\mathrm{P}} \mathrm{div}\boldsymbol{\psi}\, p_2\,\mathrm{dP} + \int_{\partial\mathrm{P}} \boldsymbol{\psi}\cdot\boldsymbol{n}\, p_2\,\mathrm{d}S + \int_{\mathrm{P}} \boldsymbol{\psi}\cdot(\boldsymbol{x}_{\mathrm{P}}\wedge\boldsymbol{p}_0)\,\mathrm{dP}\\ &= -\int_{\mathrm{P}} \mathrm{div}\boldsymbol{\psi}\, p_2\,\mathrm{dP} + \int_{\partial\mathrm{P}} \boldsymbol{\psi}\cdot\boldsymbol{n}\, p_2\,\mathrm{d}S,\end{aligned} \tag{4.16}$$

where, using (4.15) and (4.14), all the terms in the right-hand side are computable. Hence, we can define a scalar product

$$[\boldsymbol{\psi},\boldsymbol{\varphi}]_{\text{face,P}} := (\Pi_0\boldsymbol{\psi},\Pi_0\boldsymbol{\varphi})_{0,\mathrm{P}} + h_{\mathrm{P}}\sum_{f\in\partial\mathrm{P}}\int_f [(I-\Pi_0)\boldsymbol{\psi}\cdot\boldsymbol{n}][(I-\Pi_0)\boldsymbol{\varphi}\cdot\boldsymbol{n}]\,\mathrm{d}f, \tag{4.17}$$

and we again note that, assuming very mild mesh regularity conditions, for instance as in Section 5.1,

$$\alpha_1(\boldsymbol{\psi},\boldsymbol{\psi})_{0,\mathrm{P}} \le [\boldsymbol{\psi},\boldsymbol{\psi}]_{\text{face,P}} \le \alpha_2(\boldsymbol{\psi},\boldsymbol{\psi})_{0,\mathrm{P}} \qquad \forall\boldsymbol{\psi}\in V_0^{\text{face}}(\mathrm{P}) \tag{4.18}$$

for positive constants α_1,α_2 independent of h_{P}. Moreover, we also have

$$[\boldsymbol{\psi},\mathbf{p}_0]_{\text{face,P}} = \int_{\mathrm{P}} \boldsymbol{\psi}\cdot\boldsymbol{p}_0\,\mathrm{dP} = (\boldsymbol{\psi},\boldsymbol{p}_0)_{0,\mathrm{P}} \qquad \forall\boldsymbol{\psi}\in V_0^{\text{face}}(\mathrm{P}),\ \forall\boldsymbol{p}_0\in(\mathbb{P}_0(\mathrm{P}))^3. \tag{4.19}$$

Remark 4. *Using Remarks 3 and 2, by a simple dimensional count we see that the present local Nodal, Edge, and Face Virtual Element spaces coincide, whenever the element P is a tetrahedron, with the classical* $\mathbb{P}_1$*,* N_0 *and* RT_0 *elements (respectively). With a minor additional effort we could see that the same is true when P is a "rectangular box". Note that the methods do not coincide, due to a different choice of the scalar products. However, the two types of scalar products are equivalent, coincide on constants, and in practice the results are not significantly different. Hence, the present setting might be considered as a sort of "natural" extension of the* $\mathbb{P}_1$*-*N_0*-*RT_0 *approach to (much) more general element geometries.* □

4.1.4. Exact sequence properties

Here we present two important results. We first have

Proposition 4.1. *It holds*

$$\nabla V_1^{\text{node}}(\mathrm{P}) = \{\boldsymbol{v} \in V_0^{\text{edge}}(\mathrm{P}) : \ \mathbf{curl}\boldsymbol{v} = 0\}. \tag{4.20}$$

Proof. We first point out that, with the above definitions and using Proposition 3.1, for every $q \in V_1^{\text{node}}(\mathrm{P})$, we easily have that the *tangential gradient* (applied *face by face*) will belong to $V_0^{\text{edge}}(f)$. Moreover, from the definition of $V_1^{\text{node}}(\mathrm{P})$, we immediately have that $\mathbf{curl}\nabla q = 0$ and $\mathrm{div}\nabla q = \Delta q = 0$. Therefore, for any $q \in V_1^{\text{node}}(\mathrm{P})$, it holds $\nabla q \in \{\boldsymbol{v} \in V_0^{\text{edge}}(\mathrm{P}) : \ \mathbf{curl}\boldsymbol{v} = 0\}$ and thus

$$\nabla V_1^{\text{node}}(\mathrm{P}) \subseteq \{\boldsymbol{v} \in V_0^{\text{edge}}(\mathrm{P}) : \ \mathbf{curl}\boldsymbol{v} = 0\}.$$

Conversely, if $\boldsymbol{v} \in V_0^{\text{edge}}(\mathrm{P})$ with $\mathbf{curl}\boldsymbol{v} = 0$, then $\boldsymbol{v} = \nabla q$ for some $q \in H^1(\mathrm{P})$. Since, for any face $f \in \partial P$, it holds $\mathrm{rot}_f(\boldsymbol{v}_{|f}) = \mathbf{curl}\boldsymbol{v} \cdot \boldsymbol{n}_f = 0$, using Proposition 3.1 yields that q restricted to the boundary of P belongs to $V_1^{\text{node}}(\mathrm{P})_{|\partial \mathrm{P}}$. Finally, since $\mathrm{div}\boldsymbol{v} = 0$ for all $\boldsymbol{v} \in V_0^{\text{edge}}(\mathrm{P})$, we have $\Delta q = 0$. Thus q belongs to $V_1^{\text{node}}(\mathrm{P})$. □

Proposition 4.2. *It holds*

$$\mathbf{curl}\, V_0^{\text{edge}}(\mathrm{P}) := \{\boldsymbol{\psi} \in V_0^{\text{face}}(\mathrm{P}) : \ \mathrm{div}\boldsymbol{\psi} = 0\}. \tag{4.21}$$

Proof. For every $\boldsymbol{v} \in V_0^{\text{edge}}(\mathrm{P})$ we have that $\boldsymbol{\psi} := \mathbf{curl}\boldsymbol{v}$ belongs to $V_0^{\text{face}}(\mathrm{P})$. Indeed, on each face f we have that $\boldsymbol{\psi} \cdot \boldsymbol{n}_f (\equiv \mathrm{rot}_f \boldsymbol{v}_{|f})$, from (3.12) belongs to $\mathbb{P}_0(f)$ (as required in (4.13)); moreover $\mathrm{div}\boldsymbol{\psi} = 0$ (obviously) and $\mathbf{curl}\boldsymbol{\psi} \in (\mathbb{P}_0(\mathrm{P}))^3$ from (4.5). Hence,

$$\mathbf{curl}\, V_0^{\text{edge}}(\mathrm{P}) \subseteq \{\boldsymbol{\psi} \in V_0^{\text{face}}(\mathrm{P}) : \ \mathrm{div}\boldsymbol{\psi} = 0\}. \tag{4.22}$$

We show the equality of the two sets by a dimensional count. It is immediate that the condition $\mathrm{div}\boldsymbol{\psi} = 0$, for $\boldsymbol{\psi} \in V_0^{\text{face}}(\mathrm{P})$, is equivalent to

$$\sum_{f \in \partial \mathrm{P}} \int_f \boldsymbol{\psi} \cdot \boldsymbol{n}_f \, \mathrm{d}f = 0$$

and thus, recalling (4.14),

$$\dim\{\boldsymbol{\psi} \in V_0^{\text{face}}(\mathrm{P}) : \ \mathrm{div}\boldsymbol{\psi} = 0\} = N_f - 1. \tag{4.23}$$

By classical properties of linear operators, using (4.20) and finally the Euler formula on polyhedrons, we get now

$$\begin{aligned} \dim(\mathbf{curl}(V_0^{\text{edge}}(\mathrm{P}))) &= \dim(V_0^{\text{edge}}(\mathrm{P})) - \dim\{\boldsymbol{\psi} \in V_0^{\text{edge}}(\mathrm{P}) : \ \mathbf{curl}\boldsymbol{\psi} = 0\} \\ &= N_e - \dim(\nabla V_1^{node}) = N_e - (N_v - 1) = N_f - 1, \end{aligned} \tag{4.24}$$

and the result follows from (4.23) and (4.24).

□

4.2. The global spaces

Let $\mathcal{T}_h$ be a decomposition of the computational domain Ω into polyhedrons P. Again, for the time being, we assume just that all polyhedrons and all their faces are simply connected. More detailed assumptions will be presented in Section 5.1. Here we assume that

$$\textit{the permeability } \mu \textit{ is constant on each P.} \tag{4.25}$$

We define the *global spaces* as follows.

$$V_1^{\text{node}} \equiv V_1^{\text{node}}(\Omega) := \Big\{ q \in H_0^1(\Omega) \text{ such that } q_{|\mathrm{P}} \in V_1^{\text{node}}(\mathrm{P}) \, \forall \mathrm{P} \in \mathcal{T}_h \Big\}, \tag{4.26}$$

with the obvious degrees of freedom

$$\bullet \text{ for each vertex } \nu\text{: the nodal value } q(\nu). \tag{4.27}$$

For the global edge space we have

$$V_0^{\text{edge}} \equiv V_0^{\text{edge}}(\Omega) := \Big\{ \boldsymbol{v} \in H_0(\mathbf{curl}; \Omega) \text{ such that } \boldsymbol{v}_{|\mathrm{P}} \in V_0^{\text{edge}}(\mathrm{P}) \, \forall \mathrm{P} \in \mathcal{T}_h \Big\}, \tag{4.28}$$

with the obvious degrees of freedom

$$\bullet \text{ on each edge } e\text{: } \int_e \boldsymbol{v} \cdot \boldsymbol{t}_e \, \mathrm{d}e. \tag{4.29}$$

Finally, for the face space we have:

$$V_0^{\text{face}} \equiv V_0^{\text{face}}(\Omega) := \Big\{ \boldsymbol{\psi} \in H_0(\mathrm{div}; \Omega) \text{ such that } \boldsymbol{\psi}_{|\mathrm{P}} \in V_0^{\text{face}}(\mathrm{P}) \, \forall \mathrm{P} \in \mathcal{T}_h \Big\}, \tag{4.30}$$

with the degrees of freedom

$$\bullet \text{ for each face } f\text{: } \int_f \boldsymbol{\psi} \cdot \boldsymbol{n}_f \, \mathrm{d}f. \tag{4.31}$$

It is important to point out that

$$\nabla V_1^{\text{node}} \subseteq V_0^{\text{edge}}. \tag{4.32}$$

In particular, recalling the local results (4.20), it is easy to check that

$$\nabla V_1^{\text{node}} \equiv \{ \boldsymbol{v} \in V_0^{\text{edge}} \text{ such that } \mathbf{curl} \boldsymbol{v} = 0 \}. \tag{4.33}$$

Similarly, we have

$$\mathbf{curl} \, V_0^{\text{edge}} \subseteq V_0^{\text{face}}, \tag{4.34}$$

and it can be checked (recalling the local results (4.22)) that

$$\mathbf{curl} \, V_0^{\text{edge}} \equiv \{ \boldsymbol{\psi} \in V_0^{\text{face}} \text{ such that } \mathrm{div} \boldsymbol{\psi} = 0 \}. \tag{4.35}$$

Remark 5. *We point out that the inclusions* (4.32)*, and* (4.34) *are (in a sense) also* **practical***, and not only theoretical. By this, more specifically, we mean that: given the degrees of freedom of a* $q \in V_1^{\text{node}}$ *we can compute the corresponding degrees of freedom of* ∇q *in* V_0^{edge}*; and given the degrees of freedom of a* $\boldsymbol{v} \in V_0^{\text{edge}}$ *we can compute the corresponding degrees of freedom of* $\mathbf{curl}\,\boldsymbol{v}$ *in* V_0^{face}*.* □

From (4.8) we can also define a global scalar product:

$$[\boldsymbol{v}, \boldsymbol{w}]_{\text{edge}} := \sum_{\text{P}\in\mathcal{T}_h} [\boldsymbol{v}, \boldsymbol{w}]_{\text{edge,P}}. \tag{4.36}$$

We note that, recalling (4.9),

$$\alpha_*(\boldsymbol{v}, \boldsymbol{v})_{0,\Omega} \le [\boldsymbol{v}, \boldsymbol{v}]_{\text{edge}} \le \alpha^*(\boldsymbol{v}, \boldsymbol{v})_{0,\Omega} \qquad \forall \boldsymbol{v} \in V_0^{\text{edge}}. \tag{4.37}$$

It is also important to point out that, using (4.10) we have

$$[\boldsymbol{v}, \boldsymbol{p}]_{\text{edge}} = (\boldsymbol{v}, \boldsymbol{p})_{0,\Omega} := \int_\Omega \boldsymbol{v} \cdot \boldsymbol{p}\, \mathrm{d}\Omega \quad \forall \boldsymbol{v} \in V_0^{\text{edge}},\ \forall \boldsymbol{p} \text{ piecewise in } (\mathbb{P}_0)^3. \tag{4.38}$$

From (4.17) we can also define a scalar product in V_0^{face} in the obvious way

$$[\boldsymbol{\psi}, \boldsymbol{\varphi}]_{\text{face}} := \sum_{\text{P}\in\mathcal{T}_h} [\boldsymbol{\psi}, \boldsymbol{\varphi}]_{\text{face,P}} \tag{4.39}$$

and we note that

$$\alpha_1(\boldsymbol{\psi}, \boldsymbol{\psi})_{0,\Omega} \le [\boldsymbol{\psi}, \boldsymbol{\psi}]_{\text{face}} \le \alpha_2(\boldsymbol{\psi}, \boldsymbol{\psi})_{0,\Omega} \qquad \forall \boldsymbol{\psi} \in V_0^{\text{face}}. \tag{4.40}$$

It is also important to point out that, using (4.19) we have

$$[\boldsymbol{\psi}, \boldsymbol{p}]_{\text{face}} = (\boldsymbol{\psi}, \boldsymbol{p})_{0,\Omega} := \int_\Omega \boldsymbol{\psi} \cdot \boldsymbol{p}\, \mathrm{d}\Omega \qquad \forall \boldsymbol{\psi} \in V_0^{\text{face}},\ \forall \boldsymbol{p} \text{ piecewise in } (\mathbb{P}_0)^3. \tag{4.41}$$

5. Discretization of the Magneto-static Problem

We are now ready to present the discretization of our Magneto-static Problem (1.2) that we recall here:

$$\begin{cases} \text{given } \boldsymbol{j} \in H(\text{div};\Omega) \quad (\text{with } \text{div}\boldsymbol{j} = 0 \text{ in } \Omega), \quad \text{and } \mu = \mu(\boldsymbol{x}) \ge \mu_0 > 0, \\ \text{find } \boldsymbol{H} \in H_0(\mathbf{curl};\Omega) \text{ and } p \in H_0^1(\Omega) \text{ such that:} \\ \displaystyle\int_\Omega \mathbf{curl}\boldsymbol{H} \cdot \mathbf{curl}\boldsymbol{v}\, \mathrm{d}\Omega + \int_\Omega \nabla p \cdot \mu\boldsymbol{v}\, \mathrm{d}\Omega = \int_\Omega \boldsymbol{j} \cdot \mathbf{curl}\boldsymbol{v}\, \mathrm{d}\Omega \quad \forall \boldsymbol{v} \in H_0(\mathbf{curl};\Omega) \\ \displaystyle\int_\Omega \nabla q \cdot \mu\boldsymbol{H}\, \mathrm{d}\Omega = 0 \quad \forall q \in H_0^1(\Omega). \end{cases} \tag{5.1}$$

It is easy to check, by the usual theory of mixed methods, that (5.1) has a unique solution $(\boldsymbol{H}, p)$. Then we check that $\boldsymbol{H}$ and $\mu\boldsymbol{H}$ give the solution of (1.1) and $p = 0$. Checking that $p = 0$ is immediate, just taking $\boldsymbol{v} = \nabla p$ in the first equation. Once we know that $p = 0$, the first equation gives $\mathbf{curl}\boldsymbol{H} = \boldsymbol{j}$, and then the second equation gives $\text{div}\mu\boldsymbol{H} = 0$.

Remark 6. *We observe that an alternative variational formulation could be*

$$\begin{cases} \textit{given } \boldsymbol{j} \in H(\mathrm{div};\Omega) \quad (\textit{with } \mathrm{div}\boldsymbol{j} = 0 \textit{ in } \Omega), \qquad \textit{and } \mu = \mu(\boldsymbol{x}) \geq \mu_0 > 0, \\ \textit{find } \boldsymbol{H} \in H_0(\mathbf{curl};\Omega) \textit{ and } p \in H_0^1(\Omega) \textit{ such that:} \\ \displaystyle\int_\Omega \mathbf{curl}\boldsymbol{H} \cdot \mathbf{curl}\boldsymbol{v}\,\mathrm{d}\Omega + \int_\Omega \nabla p \cdot \mu\boldsymbol{v}\,\mathrm{d}\Omega = \int_\Omega \boldsymbol{j} \cdot \mathbf{curl}\boldsymbol{v}\,\mathrm{d}\Omega \quad \forall \boldsymbol{v} \in H_0(\mathbf{curl};\Omega) \\ \displaystyle\int_\Omega \nabla q \cdot \mu\boldsymbol{H}\,\mathrm{d}\Omega - \int_\Omega \nabla p \cdot \nabla q\,\mathrm{d}\Omega = 0 \quad \forall q \in H_0^1(\Omega), \end{cases} \tag{5.2}$$

or other possible variants mimicking, one way or another, the Hodge-Laplacian approach (see [4]). We observe that the discretization that we are going to introduce for (5.1) *will apply to* (5.2) *as well.*

We first construct the interpolant $\boldsymbol{j}_I \in V_0^{\mathrm{face}}$ of $\boldsymbol{j}$ that matches the degrees of freedom (4.31):

$$\bullet \text{ for each face } f\text{: } \int_f (\boldsymbol{j} - \boldsymbol{j}_I) \cdot \boldsymbol{n}_f\,\mathrm{d}f = 0. \tag{5.3}$$

From the d.o.f. (5.3) and an integration by parts it follows that

$$\int_{\mathrm{P}} \mathrm{div}(\boldsymbol{j} - \boldsymbol{j}_I)\,\mathrm{dP} = 0 \qquad \forall\,\mathrm{P} \in \mathcal{T}_h. \tag{5.4}$$

Moreover, they also imply that $\boldsymbol{j}_I \in H_0(\mathrm{div};\Omega)$ and that $\mathrm{div}\boldsymbol{j}_I = 0$ in Ω. Hence, according to (4.35), we have that $\boldsymbol{j}_I$ will be the **curl** of some $\boldsymbol{w}^* \in V_0^{\mathrm{edge}}$:

$$\exists \boldsymbol{w}^* \in V_0^{\mathrm{edge}} \text{ such that } \mathbf{curl}\boldsymbol{w}^* = \boldsymbol{j}_I. \tag{5.5}$$

Then we can introduce the **discretization** of (1.2):

$$\begin{cases} \text{find } \boldsymbol{H}_h \in V_0^{\mathrm{edge}} \text{ and } p_h \in V_1^{\mathrm{node}} \text{ such that:} \\ [\mathbf{curl}\boldsymbol{H}_h, \mathbf{curl}\boldsymbol{v}]_{\mathrm{face}} + [\nabla p_h, \mu\boldsymbol{v}]_{\mathrm{edge}} = [\boldsymbol{j}_I, \mathbf{curl}\boldsymbol{v}]_{\mathrm{face}} \quad \forall \boldsymbol{v} \in V_0^{\mathrm{edge}} \\ [\nabla q, \mu\boldsymbol{H}_h]_{\mathrm{edge}} = 0 \quad \forall q \in V_1^{\mathrm{node}}. \end{cases} \tag{5.6}$$

We point out that both $\mathbf{curl}\boldsymbol{H}_h$ and $\mathbf{curl}\boldsymbol{v}$ (as well as $\boldsymbol{j}_I$) are *face Virtual Elements in* $V_0^{\mathrm{face}}(\mathrm{P})$ in each polyhedron P, so that (taking also into account Remark 5) their *face* scalar products are computable as in (4.39). Similarly, from the degrees of freedom of a $q \in V_1^{\mathrm{node}}$ we can compute the degrees of freedom of ∇q, as an element of V_0^{edge}, so that the two edge-scalar products that appear in (5.6) are computable as in (4.36).

Proposition 5.1. *Problem* (5.6) *has a unique solution* $(\boldsymbol{H}_h, p_h)$*, and* $p_h \equiv 0$*.*

Proof. Taking $\boldsymbol{v} = \nabla p_h$ (as we did for the continuous problem (5.1)) in the first equation, and using (4.37) we easily obtain $p_h \equiv 0$ for (5.6) as well. To prove uniqueness of $\boldsymbol{H}_h$, set $\boldsymbol{j}_I = 0$, and let $\overline{\boldsymbol{H}}_h$ be the solution of the homogeneous problem. From the first equation we deduce that $\mathbf{curl}\,\overline{\boldsymbol{H}}_h = 0$. Hence, from (4.33) we have $\overline{\boldsymbol{H}}_h = \nabla q_h^*$ for some $q_h^* \in V_1^{\mathrm{node}}$. The second equation and (4.37) give then $\overline{\boldsymbol{H}}_h = 0$. □

Once we know that $p_h = 0$, the first equation of (5.6) reads

$$[\mathbf{curl}\boldsymbol{H}_h, \mathbf{curl}\boldsymbol{v}]_{\text{face}} = [\boldsymbol{j}_I, \mathbf{curl}\boldsymbol{v}]_{\text{face}} \; \forall \boldsymbol{v} \in V_0^{\text{edge}}, \tag{5.7}$$

that in view of (5.5) becomes

$$[\mathbf{curl}\boldsymbol{H}_h - \mathbf{curl}\boldsymbol{w}^*, \mathbf{curl}\boldsymbol{v}]_{\text{face}} = 0 \quad \forall \boldsymbol{v} \in V_0^{\text{edge}}. \tag{5.8}$$

Using $\boldsymbol{v} = \boldsymbol{H}_h - \boldsymbol{w}^*$ and (4.40), this easily implies

$$\mathbf{curl}\boldsymbol{H}_h = \mathbf{curl}\boldsymbol{w}^* = \boldsymbol{j}_I. \tag{5.9}$$

5.1. Error estimates

For the theoretical derivations we consider the following mesh assumptions, that are quite standard in the VEM literature. We assume the existence of a positive constant γ such that any polyhedron P (of diameter h_{P}) satisfies the following conditions:

1. P is star shaped with respect to a ball of radius bigger than γh_{P};
2. any face $f \in \partial\text{P}$ is star shaped with respect to a ball of radius bigger than γh_P, and every edge of P has length bigger than γh_{P}.

We note that condition 1 (and 2) implies that P (and any face of P) is simply connected. At the theoretical level, some of the above conditions could be avoided by using more technical arguments. At the practical level, as shown by the numerical tests of the Section 6, condition 2 is negligible since the method seems essentially impervious to degeneration of faces and edges. On the contrary, although the scheme is quite robust to distortion of the elements, condition 1 is more relevant since extremely anisotropic element shapes can lead to poor results. We also recall that we assumed μ to be piecewise constant (see (4.25)).

Let us bound the error $\boldsymbol{H} - \boldsymbol{H}_h$. We start by defining the interpolant $\boldsymbol{H}_I \in V_0^{\text{edge}}$ of $\boldsymbol{H}$, defined through the degrees of freedom (4.29):

$$\bullet \text{ on each edge } e\text{: } \int_e (\boldsymbol{H} - \boldsymbol{H}_I) \cdot \boldsymbol{t}_e \, \mathrm{d}s = 0. \tag{5.10}$$

Proposition 5.2. *With the choices* (5.3) *and* (5.10) *we have*

$$\mathbf{curl}\boldsymbol{H}_I = \boldsymbol{j}_I. \tag{5.11}$$

Proof. From (4.35) we know that $\mathbf{curl}\boldsymbol{H}_I \in V_0^{\text{face}}$. To prove (5.11) we should just show that the *face degrees of freedom* (4.31) of the difference $\mathbf{curl}\boldsymbol{H}_I - \boldsymbol{j}_I$ are zero, that is:

$$\forall f\text{: } \int_f (\mathbf{curl}\boldsymbol{H}_I - \boldsymbol{j}_I) \cdot \boldsymbol{n}_f \, \mathrm{d}f = 0. \tag{5.12}$$

Since $\boldsymbol{j} = \mathbf{curl}\boldsymbol{H}$, from the interpolation formulas (5.3) we see that

$$\forall f: \quad \int_f (\mathbf{curl}\boldsymbol{H} - \boldsymbol{j}_I) \cdot \boldsymbol{n}_f \, \mathrm{d}f = 0,$$

so that we can replace $\boldsymbol{j}_I$ with $\mathbf{curl}\boldsymbol{H}$ in (5.12), that becomes

$$\forall f: \quad \int_f \mathbf{curl}(\boldsymbol{H}_I - \boldsymbol{H}) \cdot \boldsymbol{n}_f \, \mathrm{d}f = 0. \tag{5.13}$$

Observing that (5.10) implies that

$$\int_f \mathrm{rot}_f(\boldsymbol{H} - \boldsymbol{H}_I)_{|f} \, \mathrm{d}f = 0,$$

and recalling that on each f the normal component of $\mathbf{curl}(\boldsymbol{H}_I - \boldsymbol{H})$ is equal to the rot_f of the tangential components $(\boldsymbol{H}_I - \boldsymbol{H})_{|f}$, we deduce

$$\int_f \mathbf{curl}(\boldsymbol{H}_I - \boldsymbol{H}) \cdot \boldsymbol{n}_f \, \mathrm{d}f \equiv \int_f \mathrm{rot}_f(\boldsymbol{H}_I - \boldsymbol{H})_{|f} \, \mathrm{d}f = 0.$$

Hence, (5.13) is satisfied, and the proof is concluded. □

From (5.9) and (5.11) it follows then

$$\mathbf{curl}(\boldsymbol{H}_I - \boldsymbol{H}_h) = 0 \tag{5.14}$$

and therefore, from (4.33),

$$\boldsymbol{H}_I - \boldsymbol{H}_h = \nabla q_h^* \text{ for some } q_h^* \in V_1^{\mathrm{node}}. \tag{5.15}$$

Now we define an alternative $(L^2(\Omega))^3$ inner product and norm that take into account the (piecewise constant) value of the permeability μ. We set, for $\boldsymbol{v}$ in $(L^2(\Omega))^3$,

$$\|\boldsymbol{v}\|_{0,\Omega}^2 := \int_\Omega \mu \, |\boldsymbol{v}|^2 \, \mathrm{d}\Omega. \tag{5.16}$$

When $\boldsymbol{v} = \boldsymbol{H}$ in (5.16) we get that $\|\boldsymbol{H}\|_{0,\Omega}^2 = \int_\Omega \boldsymbol{B} \cdot \boldsymbol{H} \, \mathrm{d}\Omega$, showing the connection between the new norm and the energy. We now note that, using (4.37), we have

$$\alpha_* \|\boldsymbol{H}_I - \boldsymbol{H}_h\|_{0,\Omega}^2 \leq [\boldsymbol{H}_I - \boldsymbol{H}_h, \mu(\boldsymbol{H}_I - \boldsymbol{H}_h)]_{\mathrm{edge}}, \tag{5.17}$$

and also (from (4.38) and (4.25))

$$[\boldsymbol{p}_0, \mu\boldsymbol{v}]_{\mathrm{edge}} = (\boldsymbol{p}_0, \mu\boldsymbol{v})_{0,\Omega} \quad \forall \boldsymbol{v} \in V_0^{edge} \text{ and } \forall \boldsymbol{p}_0 \text{ piecewise constant vector.} \tag{5.18}$$

Then, starting with (5.17) we have:

$$
\begin{aligned}
\alpha_* \|\!|\boldsymbol{H}_I - \boldsymbol{H}_h|\!\|_{0,\Omega}^2 &\leq [\boldsymbol{H}_I - \boldsymbol{H}_h, \mu(\boldsymbol{H}_I - \boldsymbol{H}_h)]_{\text{edge}} \\
&= \text{(using (5.15))}\ [\boldsymbol{H}_I - \boldsymbol{H}_h, \mu\nabla q_h^*]_{\text{edge}} \\
&= \text{(using the second of (5.6))}\ [\boldsymbol{H}_I, \mu\nabla q_h^*]_{\text{edge}} \\
&= \text{(adding and subtracting } \Pi_0\boldsymbol{H})\ [\boldsymbol{H}_I - \Pi_0\boldsymbol{H}, \mu\nabla q_h^*]_{\text{edge}} + [\Pi_0\boldsymbol{H}, \mu\nabla q_h^*]_{\text{edge}} \\
&= \text{(using (5.18))}\ [\boldsymbol{H}_I - \Pi_0\boldsymbol{H}, \mu\nabla q_h^*]_{\text{edge}} + (\Pi_0\boldsymbol{H}, \mu\nabla q_h^*)_{0,\Omega} \\
&= \text{(adding and subtracting } \boldsymbol{H})\ [\boldsymbol{H}_I - \Pi_0\boldsymbol{H}, \mu\nabla q_h^*]_{\text{edge}} + (\Pi_0\boldsymbol{H} - \boldsymbol{H}, \mu\nabla q_h^*)_{0,\Omega} + (\boldsymbol{H}, \mu\nabla q_h^*)_{0,\Omega} \\
&= \text{(from the second of (1.2))}\ [\boldsymbol{H}_I - \Pi_0\boldsymbol{H}, \mu\nabla q_h^*]_{\text{edge}} + (\Pi_0\boldsymbol{H} - \boldsymbol{H}, \mu\nabla q_h^*)_{0,\Omega} \\
&\leq \text{(using Cauchy-Schwarz and (4.37))}\ \left(\alpha^* \|\!|\boldsymbol{H}_I - \Pi_0\boldsymbol{H}|\!\|_{0,\Omega} + \|\!|\Pi_0\boldsymbol{H} - \boldsymbol{H}|\!\|_{0,\Omega}\right) \|\!|\nabla q_h^*|\!\|_{0,\Omega} \\
&\leq \text{(using again (5.15))}\ \left(\alpha^* \|\!|\boldsymbol{H}_I - \Pi_0\boldsymbol{H}|\!\|_{0,\Omega} + \|\!|\Pi_0\boldsymbol{H} - \boldsymbol{H}|\!\|_{0,\Omega}\right) \|\!|\boldsymbol{H}_I - \boldsymbol{H}_h|\!\|_{0,\Omega}
\end{aligned}
$$

that implies immediately (since $\alpha^* \geq 1$)

$$
\|\!|\boldsymbol{H}_I - \boldsymbol{H}_h|\!\|_{0,\Omega} \leq \frac{\alpha^*}{\alpha_*}(\|\!|\boldsymbol{H}_I - \Pi_0\boldsymbol{H}|\!\|_{0,\Omega} + \|\!|\Pi_0\boldsymbol{H} - \boldsymbol{H}|\!\|_{0,\Omega}). \tag{5.19}
$$

We can summarize the result in the following theorem.

Theorem 5.3. *Problem* (5.6) *has a unique solution and the following estimate holds:*

$$
\|\!|\boldsymbol{H} - \boldsymbol{H}_h|\!\|_{0,\Omega} \leq C \left(\|\!|\boldsymbol{H} - \boldsymbol{H}_I|\!\|_{0,\Omega} + \|\!|\boldsymbol{H} - \Pi_0\boldsymbol{H}|\!\|_{0,\Omega}\right), \tag{5.20}
$$

with C a constant independent of the mesh size. Moreover, thanks to (5.9) *we also have*

$$
\|\mathbf{curl}(\boldsymbol{H} - \boldsymbol{H}_h)\|_{0,\Omega} = \|\boldsymbol{j} - \boldsymbol{j}_I\|_{0,\Omega}. \tag{5.21}
$$

The above result can be combined with standard polynomial approximation estimates on star shaped polyhedra in order to estimate the terms involving the L^2 projection on polynomials. Moreover, approximation estimates for the VEM interpolants $\boldsymbol{H}_I$ and $\boldsymbol{j}_I$ can be derived (under the mesh assumptions at the beginning of this section) by an extension of the arguments in [12], [11], [15], [24]. We therefore obtain, provided that $\boldsymbol{H}$ and $\boldsymbol{j}$ are sufficiently regular,

$$
\|\!|\boldsymbol{H} - \boldsymbol{H}_h|\!\|_{0,\Omega} \leq Ch \qquad \|\mathbf{curl}(\boldsymbol{H} - \boldsymbol{H}_h)\|_{0,\Omega} \leq Ch.
$$

6. Numerical results

In this section we provide some numerical results. We first provide a test on a polyhedral domain with Dirichlet boundary data, then a test on a cylindrical domain with jumping coefficients and Neumann boundary data, and finally a benchmark example with a more complex geometry.

6.1. Test case 1: h-analysis with homogeneous Dirichlet boundary conditions

In this subsection we set $\mu = 1$ and take as exact solution of (1.1) the vector field

$$\boldsymbol{H}(x,\, y,\, z) := \frac{1}{\pi} \begin{pmatrix} \sin(\pi y) - \sin(\pi z) \\ \sin(\pi z) - \sin(\pi x) \\ \sin(\pi x) - \sin(\pi y) \end{pmatrix} .$$

We consider as domain Ω the truncated octahedron [28] and three different discretizations, see Fig. 1:

- **Structured**, a mesh composed by structured cubes inside Ω and arbitrarily shaped elements close to the boundary;
- **CVT**, a Centroidal Voronoi Tessellation of Ω obtained via a standard Lloyd algorithm [19];
- **Random**, a mesh obtained by the constrained Voronoi Tessellation of points randomly put inside Ω.

The first type of mesh can be generated by using a Voronoi generation algorithm with seeds disposed in a regular formation, see [5]. This approach allows to approximate complex geometries and still inherits many among the computational advantages of regular cubical meshes. The last type of meshes is instead interesting in order to check the robustness of the method, since it exhibits edges and faces (see the details in Fig. 1) that can be very small with respect to the size of the parent element. To get such discretizations, we use the c++ library `voro++` [25].

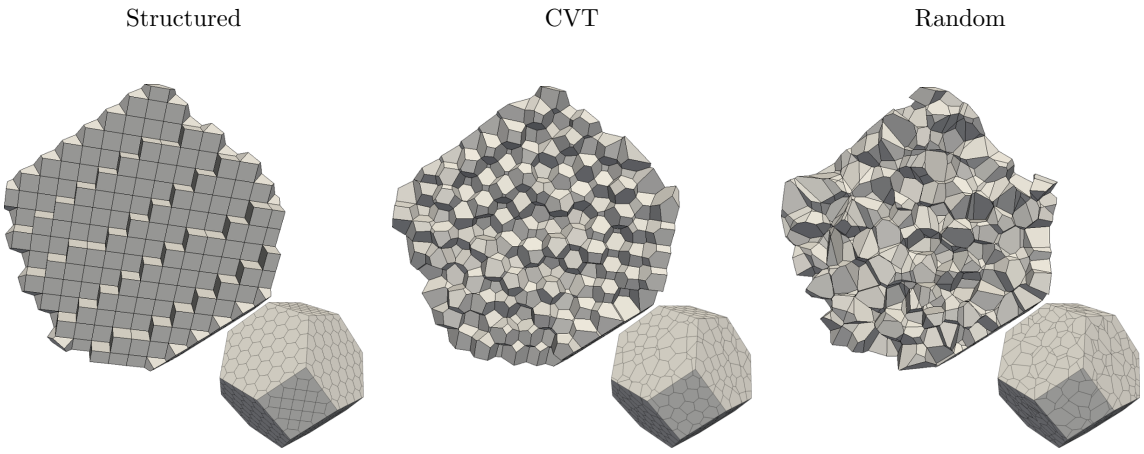

Figure 1: Three different discretizations of the truncated octahedron.

We associate to each mesh a mesh-size h defined as

$$h := \frac{1}{N_P} \sum_{i=1}^{N_P} h_P \,,$$

where N_P is the number of polyhedrons in the mesh and h_P is the diameter of the polyhedron P. We compute the L^2-error on $\boldsymbol{H}$ as

$$\frac{||\boldsymbol{H} - \Pi_0 \boldsymbol{H}_h||_{0,\Omega}}{||\boldsymbol{H}||_{0,\Omega}},$$

where $\Pi_0 \boldsymbol{H}_h$ is the piecewise constant projection of $\boldsymbol{H}_h$ defined in (4.7). Fig. 2 (left) shows the convergence rate for each type of mesh. The slopes are coherent with the theory, see Equation (5.20). Moreover, from this graph we can better appreciate the robustness of the VEM with respect to element distortions. Indeed, the convergence lines for the three meshes are very close to each other.

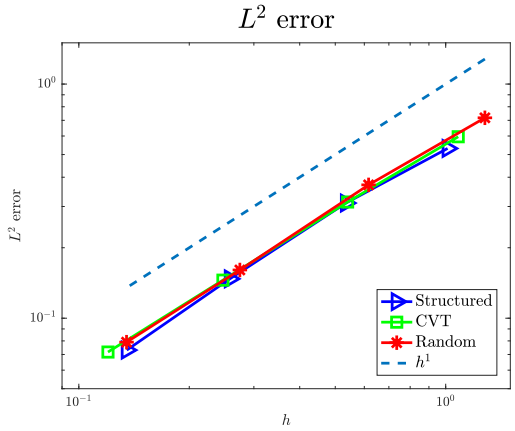

$l^\infty-$norm

step	Structured	CVT	Random
1	1.5098e-15	1.1844e-15	4.7323e-13
2	7.0101e-16	2.5902e-14	1.6107e-12
3	2.6762e-15	1.0476e-13	1.8733e-10
4	7.0545e-15	1.0953e-10	1.0001e-07

Figure 2: Test case 1: L^2-error for $\boldsymbol{H}$ (left), and $l^\infty-$norm of $dof(p_h)$ (right).

The results for the Lagrange multiplier p_h are shown in Fig. 2 (right). As shown in Section 5, the exact solution p_h of the discrete problem is identically zero. Clearly, the roundoff errors generate, out of the computer, a p_h that is *almost* identically zero. In some sense we could then take the value of the *computed* p_h as a measure (or, better, a rough indicator) of the conditioning of the final linear system. In particular we see that the Random meshes generate a worse conditioning.

6.2. Test case 2: discontinuous μ and homogeneous Neumann conditions

In this subsection we consider an example taken from [14]. The geometry consists in a cylindrical domain with two concentric connected components, $\mathcal{S}_1$ and $\mathcal{S}_2$, separated by a magnetic material, $\mathcal{M}$ (see a cross-section in Fig. 3). A current of the same intensity I =70 000A but opposite direction passes along $\mathcal{S}_1$ and $\mathcal{S}_2$. We assign the following current intensity (with $\mathbf{e}_z := (0,\, 0,\, 1)^t$)

$$\boldsymbol{j}(x,\, y,\, z) := \begin{cases} \dfrac{I}{\pi a^2}\, \mathbf{e}_z & \text{if } \boldsymbol{x} \in \mathcal{S}_1 \\ \mathbf{0} & \text{if } \boldsymbol{x} \in \mathcal{M} \\ -\dfrac{I}{\pi(c^2 - b^2)}\, \mathbf{e}_z & \text{if } \boldsymbol{x} \in \mathcal{S}_2. \end{cases} \tag{6.1}$$

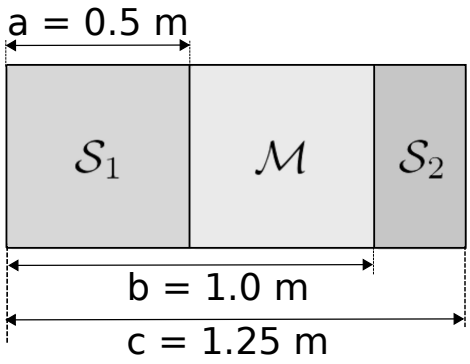

Figure 3: Test case 2: meridian cross section of the computational domain.

We apply homogeneous Neumann boundary conditions and we set $\mu_{\mathcal{S}_1} = \mu_{\mathcal{S}_2} = 1.0$, $\mu_{\mathcal{M}} = 1000.0$. Then the exact solution is given by

$$\boldsymbol{H}(x,\, y,\, z) := \begin{cases} \dfrac{I}{2\pi a^2}\, \mathbf{e}_\theta & \text{if } \boldsymbol{x} \in \mathcal{S}_1 \\ \dfrac{I}{2\pi r^2}\, \mathbf{e}_\theta & \text{if } \boldsymbol{x} \in \mathcal{M} \\ \left[-\dfrac{I}{2\pi(c^2-b^2)} + \dfrac{1}{r^2}\left(\dfrac{I}{2\pi} + \dfrac{Ib^2}{2\pi(c^2-b^2)} \right) \right] \mathbf{e}_\theta & \text{if } \boldsymbol{x} \in \mathcal{S}_2 \end{cases} \tag{6.2}$$

where $\mathbf{e}_\theta := (-y,\, x,\, 0)^t$, $r = \sqrt{x^2+y^2}$ and $a = 0.5, b = 1, c = 1.25$ (see Fig. 3).

To deal with Neumann boundary conditions, problem (5.1) must be modified, looking for $\boldsymbol{H} \in H(\mathbf{curl}; \Omega)$ and $p \in H^1(\Omega)$. The magnetic field $\boldsymbol{H}$ will still be unique, while p will be determined only up to a constant. In the code the constant is fixed by requiring the average of the vertex values of p_h to be zero.

We build two meshes of the cylinder by extruding two planar two-dimensional meshes: one made of polygons [27] and one made of triangles [26]. We refer to the former as voro-extrusion and to the latter as tria-extrusion (for an example of both see Fig. 4). Then we make two sets of meshes with decreasing mesh-size. In Fig. 5 we depict the convergence curves on the left, and on the right we provide the $l^\infty-$norm of the vectors $dof(p_h)$. Both quantities behave as expected: indeed, we get a convergence rate equal to 1, for the L^2 error on the vector field $\boldsymbol{H}_h$, while the values of $l^\infty-$norm vanish up to machine algebra errors.

6.3. Test case 3: a cylindrical electromagnet

In this subsection we consider a typical benchmark problem, see e.g. [13, 14, 20]. The geometry consists in a ferromagnetic cylindrical core, $\mathcal{C}$, surrounded by a toroidal coil with a rectangular cross section, $\mathcal{T}$, with air, $\mathcal{A}$, around these two structures. In Fig. 6 we show a meridian cross section of the domain where we specify the dimensions of the cylindrical core, the toroidal coil and the bounding box of the domain.

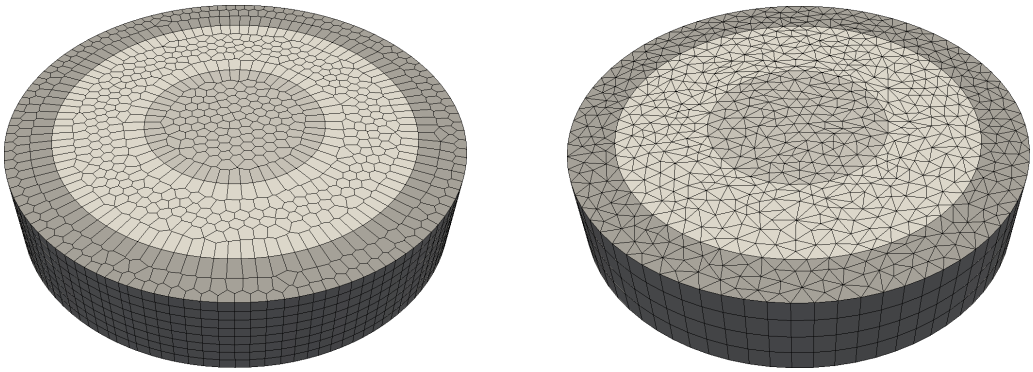

Figure 4: Test case 2: two polyhedral decompositions of the cylinder: voro-extrusion (left), and tria-extrusion (right).

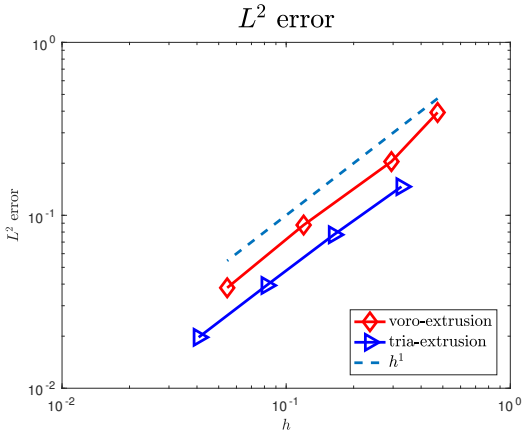

	$l^\infty-$norm	
step	voro-extrusion	tria-extrusion
1	2.1273e-11	1.3632e-10
2	1.0564e-10	4.1360e-10
3	1.4887e-10	1.0027e-09
4	4.5312e-10	1.1151e-08

Figure 5: Test case 2: L^2 error for $\boldsymbol{H}$ (left), and $l^\infty-$norm of $dof(p_h)$ (right).

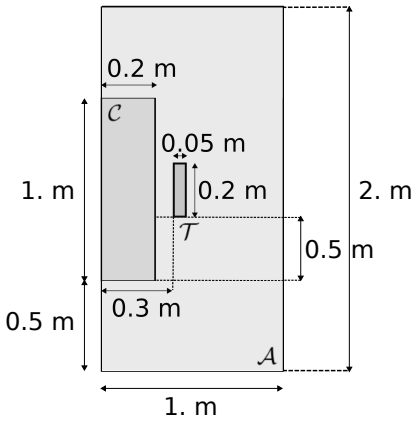

Figure 6: Test case 3: meridian cross section of the computational domain.

One looks for the magnetic flux generated by a constant current passing along the toroidal coil. More specifically, we assume a constant current of 1 Ampère, i.e.,

$$\boldsymbol{j}(x,\, y,\, z) := \begin{cases} \dfrac{1}{A|\mathbf{e}_\theta|}\,\mathbf{e}_\theta & \text{if } \boldsymbol{x} \in \mathcal{T} \\ \mathbf{0} & \text{otherwise} \end{cases}$$

where $\mathbf{e}_\theta = (-y,\, x,\, 0)^t$, $|\mathbf{e}_\theta|$ denotes the norm of $\mathbf{e}_\theta$ and A is the area of the cross section of the coil. The relative magnetic permeability is taken as: $\mu_{\mathcal{T}} = 1.0$ for the coil, $\mu_{\mathcal{C}} = 10000.0$ in the ferromagnetic core, and $\mu_{\mathcal{A}} = 1.0$ for the air. Moreover, we suppose that the artificial boundary is sufficiently far from both the ferromagnetic cylinder and the toroidal core so that we can apply the Neumann boundary conditions $\boldsymbol{H} \cdot \boldsymbol{n} = 0$.

In Fig. 7 we show one of the meshes used in this example. Here too the meshes are constructed by extruding two-dimensional ones. Figs. 8 and 9 show a qualitative comparison between the solution provided

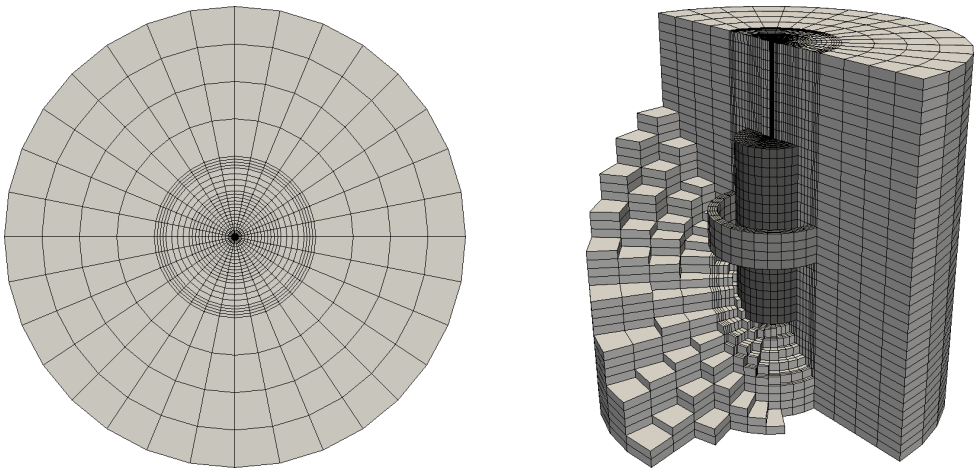

Figure 7: Test case 3: On the right a clip of the 3d mesh obtained extruding the 2d mesh on the left.

in [13] (left), and that obtained by the present method (right). More specifically, in Fig. 8, we show the modulus of the magnetic flux density, i.e. the modulus of $\boldsymbol{B} = \mu\boldsymbol{H}$, inside the cylindrical core. Then, in Fig. 9 we show $\boldsymbol{B}$ along some cross sections of the cylindrical core and the toroidal coil. In both cases the results of two methods show a comparable behavior.

Finally, to have a more quantitative validation of this example, we compute the so-called magnetic energy

$$W := \int_{\mathcal{D}} \boldsymbol{B} \cdot \boldsymbol{H}\ \mathrm{d}\Omega = \int_{\mathcal{D}} \mu|\boldsymbol{H}|^2\ \mathrm{d}\Omega\,,$$

for each sub-domain $\mathcal{C}$, $\mathcal{T}$ and $\mathcal{A}$ (see also (5.16)). We consider a sequence of three nested meshes to verify

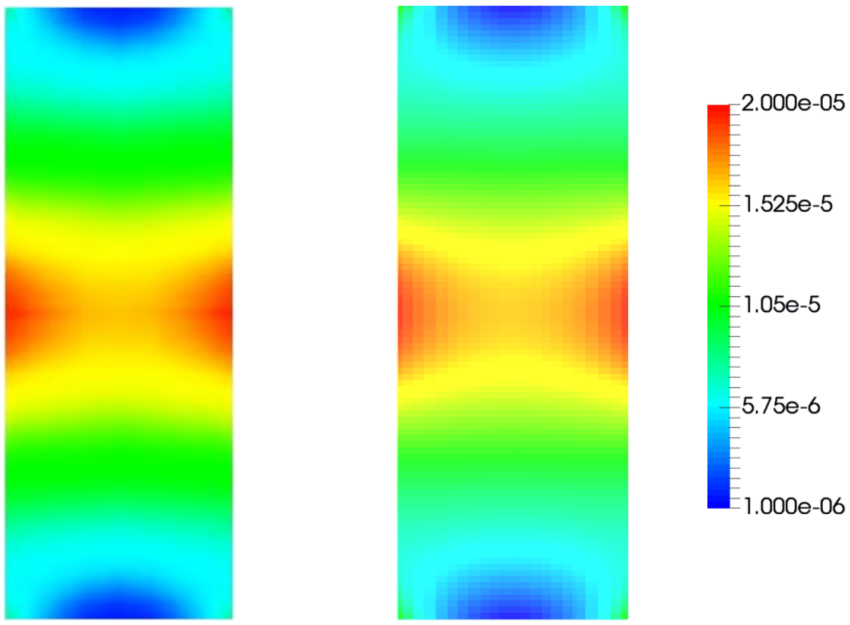

Figure 8: Test case 3: $|\boldsymbol{B}|$ in a section of $\mathcal{C}$: from [13] (left) and that from the present approach (right).

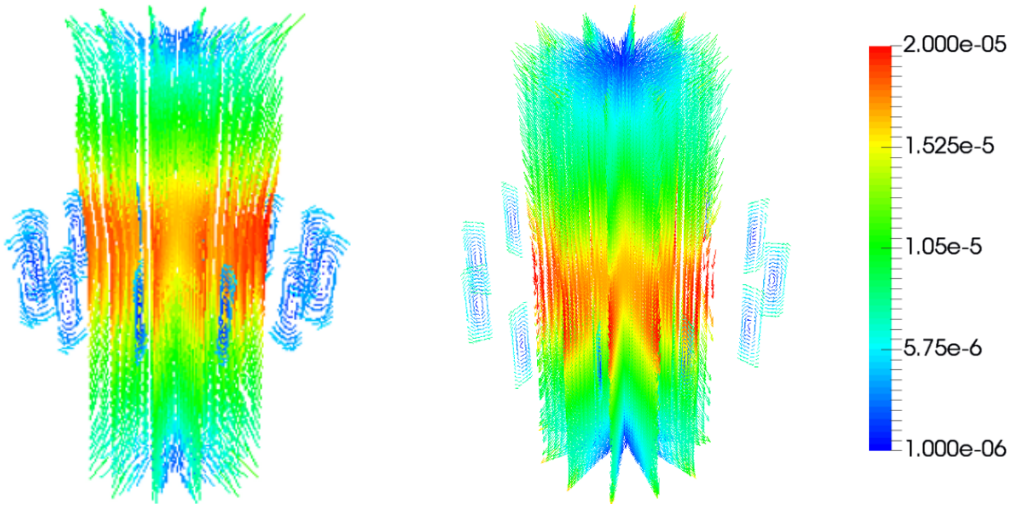

Figure 9: Test case 3: $\boldsymbol{B}$ in a section of $\mathcal{C}$ and $\mathcal{T}$: from [13] (left), and from the present approach (right).

the convergence rate of these energies. We refer to these meshes as mesh1, mesh2 and mesh3, the first mesh being the coarsest.

Since we do not have the exact solution of this problem, in order to assess the accuracy of our results for the magnetic energy W we proceed as in [14], i.e. we consider as exact values of the magnetic energies the values obtained by the software *FLUX2D* on a very fine mesh. The numerical solution of *FLUX2D* follows a scalar potential formulation and exploits the symmetry of the domain via a two-dimensional cylindric coordinate system. The data are collected in Table 1 and in parenthesis we show the relative error. The method behaves as expected.

W in	$\mathcal{A}$		$\mathcal{C}$		$\mathcal{T}$	
FLUX2D	9.09e-07		4.73e-10		3.61e-08	
mesh1 VEM	9.70e-07	(6.7%)	7.54e-10	(59.4%)	3.29e-08	(8.8%)
mesh2 VEM	9.22e-07	(1.4%)	5.53e-10	(16.9%)	3.81e-08	(5.5%)
mesh3 VEM	9.11e-07	(0.2%)	4.98e-10	(5.2%)	3.75e-08	(3.8%)

Table 1: Test case 3: Behavior of W, in the three regions, computed with the present method

Acknowledgments

The first and third authors were partially supported by the European Research Council through the H2020 Consolidator Grant (grant no. 681162) CAVE – Challenges and Advancements in Virtual Elements. This support is gratefully acknowledged.

References

[1] B. Ahmad, A. Alsaedi, F. Brezzi, L. D. Marini, and A. Russo, *Equivalent projectors for virtual element methods*, Comput. Math. Appl. **66** (2013), no. 3, 376–391.

[2] D.N. Arnold, D. Boffi, and R.S. Falk, *Approximation by quadrilateral finite elements*, Math. Comp. **71** (2002), no. 239, 909–922.

[3] ———, *Quadrilateral H(div) finite elements*, SIAM J. Numer. Anal. **42** (2005), no. 6, 2429–2451.

[4] D.N. Arnold, R.S. Falk, and R. Winther, *Finite element exterior calculus, homological techniques, and applications*, Acta Numer. **15** (2006), 1–155.

[5] L. Beirão da Veiga, F. Dassi, and A. Russo, *High-order virtual element method on polyhedral meshes*, Computers & Mathematics with Applications (2017).

[6] L. Beirão da Veiga, F. Brezzi, A. Cangiani, G. Manzini, L. D. Marini, and A. Russo, *Basic principles of virtual element methods*, Math. Models Methods Appl. Sci. **23** (2013), no. 1, 199–214.

[7] L. Beirão da Veiga, F. Brezzi, F. Dassi, L. D. Marini, and A. Russo, *Virtual element approximation of 2d magnetostatic problems*, Comput. Methods Appl. Mech. Engrg. (2017), http://dx.doi.org/10.1016/j.cma.2017.08.013.

[8] L. Beirão da Veiga, F. Brezzi, L. D. Marini, and A. Russo, *$H(div)$ and $H(curl)$-conforming VEM*, Numer. Math. **133** (2016), no. 2, 303–332.

[9] ———, *Serendipity nodal VEM spaces*, Comp. Fluids **141** (2016), 2–12.

[10] ———, *Serendipity face and edge VEM spaces*, Rend. Lincei Mat. Appl. **28** (2017), no. 1, 143–180.

[11] L. Beirão da Veiga, C. Lovadina, and A. Russo, *Stability analysis for the virtual element method*, Math. Models Methods Appl. Sci. (2017), 10.1142/S021820251750052X.

[12] L. Beirão da Veiga, D. Mora, G. Rivera, and R. Rodríguez, *A virtual element method for the acoustic vibration problem*, Numerische Mathematik **136** (2017), 725–736.

[13] A. Bermúdez, D. Gómez, and P. Salgado, *Mathematical models and numerical simulation in electromagnetism*, Unitext, vol. 74, Springer, 2014.

[14] A. Bermúdez, R. Rodríguez, and P. Salgado, *A finite element method for the magnetostatic problem in terms of scalar potentials*, SIAM Journal on Numerical Analysis **46** (2008), no. 3, 1338–1363.

[15] S. Brenner, Q. Guan, and L. Sung, *Some estimates for virtual element methods*, Computational Methods in Applied Mathematics, doi:10.1515/cmam-2017-0008, 2017.

[16] F. Brezzi and A. Buffa, *Innovative mimetic discretizations for electromagnetic problems*, J. Comput. Appl. Math **234** (2010), 1980–1987.

[17] B. Cockburn, D. Di Pietro, and A. Alexandre Ern, *Bridging the hybrid high-order and hybridizable discontinuous galerkin methods*, ESAIM Math. Model. Numer. Anal. **50** (2016), 635–650.

[18] L. Demkowicz, J. Kurtz, D. Pardo, M. Paszenski, W. Rachowicz, and A. Zdunek, *Computing with hp-adaptive finite elements. vol. 2. frontiers: Three dimensional elliptic and maxwell problems with applications*, Applied Mathematics and Nonlinear Science, Chapman & Hall/CRC, Boca Raton, 2008.

[19] Qiang Du, V. Faber, and M. Gunzburger, *Centroidal voronoi tessellations: Applications and algorithms*, SIAM Rev. **41** (1999), no. 4, 637–676.

[20] M. Fontana, *Adaptive finite element computation of 3D magnetostatic problems in potential formulation*, Tech. Report Preprint 2001-8, University of Chalmers, Göteborg, 2001.

[21] H. Kanayama, R. Motoyama, K. Endo, and F. Kikuchi, *Three dimensional magnetostatic analysis using nedelec's elements*, IEEE Transactions on Magnetics **26** (1990), 682–685.

[22] K. Lipnikov, G. Manzini, F. Brezzi, and A. Buffa, *The mimetic finite difference method for the 3d magnetostatic field problems on polyhedral meshes*, J. Comput. Phys. **230** (2011), 305–328.

[23] P. Monk, *Finite element methods for Maxwell's equations*, Numerical Mathematics and Scientific Computation, Oxford University Press, New York, 2003.

[24] D. Mora, G. Rivera, and R. Rodríguez, *A virtual element method for the Steklov eigenvalue problem*, Math. Models Methods Appl. Sci. **25** (2015), no. 8, 1421–1445.

[25] C.H. Rycroft, *Voro++: A three-dimensional voronoi cell library in c++*, Chaos **19** (2009), no. 4, 041111.

[26] J.R. Shewchuk, *Triangle: Engineering a 2d quality mesh generator and delaunay triangulator*, Applied computational geometry towards geometric engineering, Springer, 1996, pp. 203–222.

[27] C. Talischi, G.H. Paulino, A. Pereira, and I.FM Menezes, *Polymesher: a general-purpose mesh generator for polygonal elements written in matlab*, Structural and Multidisciplinary Optimization **45** (2012), no. 3, 309–328.

[28] R. Williams, *The geometrical foundation of natural structure: A source book of design*, Dover Publications, 1979.